Model for coarsening froths and foams

Henrik Flyvbjerg*
CONNECT, The Niels Bohr Institute, Blegdamsvej 17, DK-2100 Copenhagen Ø, Denmark
(Received 25 September 1992)

The coarsening process of froths and foams is described statistically in two dimensions by a "random neighbor model." This nonlinear dynamical model contains no free parameters; all rates are determined dynamically. It describes normal growth, agrees with experimental results, throws light on old data, and, hopefully, inspires new simulations and measurements. Lewis's law [Anat. Rec. **38**, 341 (1928); Am. J. Bot. **30**, 74 (1943)], and some other properties, can be derived analytically from the model.

PACS number(s): 05.70.Ln, 64.60.My, 68.90.+g, 82.70.Rr

I. INTRODUCTION

Soap froths and related physical systems have recently been investigated in very nice experiments [1–15] and simulations [14–26]. The progress on the theoretical side has been more scant [27–33], and a comprehensive theory for froths, foams, and related domain boundary networks is still missing. This is not to say that models for these systems have not been suggested. The subject is believed to have its conceptual equivalent to the ideal gas, Ising model, and hydrogen atom in the ideal, dry soap froth, which is believed to contain the quintessential physics of a number of interesting problems in material science, geology, biology, ...; see [34], [35], and [36] for reviews. But in contrast to the Ising model and the hydrogen atom, the dynamics of the ideal froth has not been finally defined, let alone solved, not even in two dimensions, where von Neumann's law (see below) acts as a local decoupling theorem. So for lack of better, computer simulations have taken over the role of real theory in the discussion of experiments; see, for example, Ref. [11].

But simulations are in a sense experiments themselves, albeit ideal ones. Even when they reproduced experimental results perfectly, they only provide us with an algorithm, not an *understanding* in terms of a few, well-understood principles. This, then, is where more simplistic models become useful. In the construction of such models, we ignore the system's less important properties, and construct a more transparent description in terms of the important ones. Which properties are what, we decide ourselves, with an eye on the model's ability to describe results from experiments and simulations.

In the model presented and solved below, a froth's physical forces, unavoidable geometrical constraints, and spatial disorder are considered important for the dynamics of its individual bubbles. Correlations between properties of individual bubbles are judged unimportant and neglected. The model thus arrived at is transparent in its workings, contains no free parameters, and reproduces experimental and simulation data well. It should be seen as a minimal model: it was constructed with the minimum number of properties necessary to yield reasonable results. More properties may be added to refine the model and make its predictions agree even better with experimental results. This is discussed at some length, but not done, in the present paper. The model and preliminary results for its solution were briefly described in [30] and [37].

Section II below describes the system to be modeled. Section III describes the model. Section IV describes the model in scale-invariant form and the "normal growth" following from it. Section V describes how the model was solved numerically. Section VI presents the solution in various ways. Sections VII–X describe various aspects of the solution, and derive some of them analytically: the topological distribution in Sec. VII, moments of this distribution in Sec. VIII, Lewis's law in Sec. IX, and the area distribution in Sec. X. Section XI discusses one of the two approximations, we have done, when defining the model. Section XII concludes on what we have learned, points out some challenges for simulations and experiments, and suggests some ways to extend the model. Some questions of interest for further model building, which may be answered by simulations and experiments, are also given. Appendix A collects our notation, which is introduced wherever needed throughout the paper. Appendix B describes an analytical, ansatz-based, approach to the model's solution.

II. THE IDEAL, DRY FROTH IN TWO DIMENSIONS

A froth has two kinds of dynamics, a fast and a slow. On the short-time scale, it is a disordered systems with an infinity of stable states. On the long-time scale, it is a deterministic system with a relaxation dynamics that may be as sensitive to initial data as chaotic systems are, and with no stable state. After the instantaneous settling of a froth in one of its multitude of stable states, the slow dynamics may be observed: The pressure difference between neighbor bubbles causes diffusion of air molecules

through the film forming the wall between bubbles. This process takes the froth through a continuous series of states, which are stable with respect to the fast dynamics. Figure 1 shows two time series for two-dimensional dry froths, photocopied by Glazier, Gross, and Stavans at intervals of several hours [38]. The two-dimensional froths were formed from three-dimensional froths caught between two glass plates. They are called dry when the film between bubbles has been drained of excess liquid to its minimal thickness, is homogenous throughout the froth, and much thinner than the typical bubble diameter. The froths clearly coarsen with time.

The mechanism of coarsening is easy to understand: in two dimensions, bubble walls in a dry froth are sections of circles that join three at a time at 120° angles. The angles are necessarily 120° in order for the tensions of the three joining walls to balance each other, rendering the froth static with respect to its fast dynamics. Thus few-sided bubbles must have walls that curve outward. That requires excess pressure relatively to the neighbors in such bubbles. Consequently air slowly diffuses through the walls to the neighbors, and few-sided bubbles *shrink* in time, to vanish, eventually, with a larger average bubble size as result.

In two dimensions, simple geometrical arguments lead to von Neumann's law for the rate of change with time t of the area A of any bubble with n neighbors [39],

$$\frac{dA}{dt} = v_n = v_7(n-6), \qquad v_7 = \frac{\pi}{3}\sigma\tau \tag{1}$$

(von Neumann's law), where σ is the constant of diffusion through the bubble walls, τ is the tension in the walls, and the area A of the bubble is the two-dimensional equivalent of its volume. Notice that the rate of change of the area depends on only *one* property of the bubble, its number of neighbors n, which is also called its *topological class*, or its *topology*.

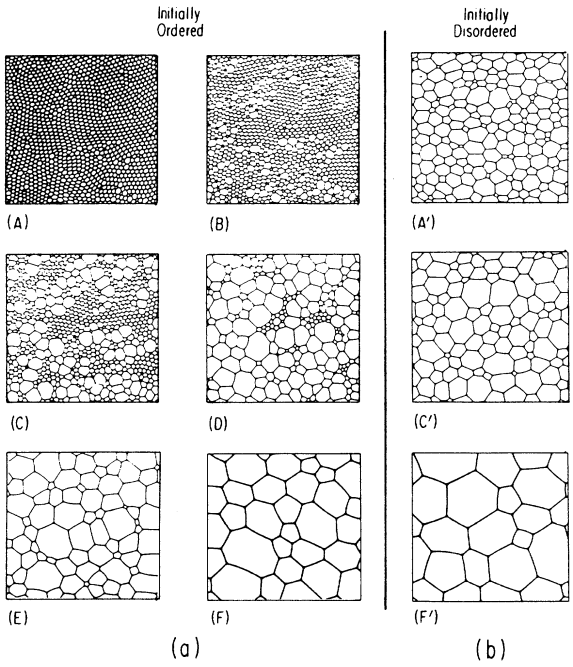

FIG. 1. Evolution of (a) initially ordered and (b) initially disordered soap froths in 2D [38]. Photos were taken after 1 h, 2.52 h, 4.82 h, 8.63 h, 19.87 h, and 52.33 h for series (a), and after 1.95 h, 21.50 h, and 166.15 h for the series (b).

Bubbles with topology $n < 6$ shrink according to von Neumann's law. When a bubble has shrunk to zero area, it has disappeared from the froth, and thereby changed the number of neighbors of some of its neighbors; see Fig. 2(a). Figure 2(b) shows a different process, *neighbor switching*, which also changes the number of neighbors to the bubbles involved. We shall neglect these so-called T_1 processes in the present paper because those that are not related to the vanishing of bubbles are responsible for less than 1% of the topology changing processes, according to experimental observations [38]. Those T_1 processes that *are* related to the vanishing of bubbles occur frequently [38]; but their net effect might be negligible; see Sec. XI. So, effectively we have no explicit T_1 processes in our model. This is our first approximation. It keeps our model simple. So simple that it will contain no free parameters.

From Euler's theorem for the plane follows that the average number of neighbors to a bubble is 6. The vanishing processes sketched in Fig. 2(a) respect this theorem by conserving the average value 6: a vanishing bubble has less than six neighbors; its deficit, $6-n$, is transferred to its neighbors in the vanishing process, thereby keeping constant an average equal to 6. For example, when a bubble with topology 5 disappears, two of its neighbors lose an edge, and one gains one.

The correct description of how these vanishing processes affect the ensemble of bubbles involves neighbor correlations. Nearest-neighbor correlations are expressed in Aboav-Weaire's law,

$$m(n) = 6 - a + (6a + \mu_2)/n \quad \text{(Aboav-Weaire's law)}, \tag{2}$$

where $m(n)$ is the average topology of nearest neighbors to bubbles with topology n, a is a constant of order 1, and μ_2, defined below, is the second moment of the distribution of n, [40–44]. Experiments and simulations give $\mu_2 \simeq 1.4-1.5$ [36] and $\mu_2 \simeq 1.2$ [25]. As our second and last approximation we neglect all neighbor correlations, effectively replacing $m(n)$ with $m(6)$ for vanishing bubbles. This approximation is worse for bubbles with fewer sides. But because they turn out to be rare, our results turn out quite well.

III. THE RANDOM-NEIGHBOR MODEL

Let $p_n(A;t)$ denote the froth's relative frequency of bubbles with area A and topology n at time t. A notation for the frequency of bubbles with topology n and any area will also be useful,

$$P_n(t) = \int_0^\infty dA\, p_n(A;t). \tag{3}$$

The time evolution of $p_n(A;t)$ is partially determined by von Neumann's law,

$$\left(\frac{\partial}{\partial t}+v_n\frac{\partial}{\partial A}\right)p_n(A;t)=\mathcal{S}, \tag{4}$$

where the right-hand side $\mathcal{S}$ must describe the consequences of the fact that bubbles with $n<6$ disappear from the ensemble when their areas vanish. It is found as follows.

Since the soap froth is space filling, when the number $\mathcal{N}$ of bubbles in some fixed reference area $\mathcal{A}$ decreases, the average area $\bar{A}$ of bubbles within the reference area must increase,

$$\mathcal{A}=\mathcal{N}\bar{A}\Rightarrow\dot{\bar{A}}/\bar{A}=-\dot{\mathcal{N}}/\mathcal{N}. \tag{5}$$

The rate at which bubbles disappear is

$$|\dot{\mathcal{N}}|/\mathcal{N}=\sum_{k=0}^{5}|v_k|\,p_k(0;t).$$

This disappearance of some bubbles increases the probability for the remaining bubbles. Consequently, the right-hand side of Eq. (4) must contain an additive term

$$\left(\sum_{k=0}^{5}|v_k|\,p_k(0;t)\right)p_n(A;t)=\dot{\bar{A}}/\bar{A}\,p_n(A;t).$$

This term assures conservation of probability,

$$\sum_n\int_0^\infty dA\,p_n(A;t)=\sum_n P_n(t)=1. \tag{6}$$

As pointed out in Sec. II, the vanishing processes sketched in Fig. 2(a) respect Euler's theorem for the plane, the average topology is 6, and conserved,

$$\sum_n n\int_0^\infty dA\,p_n(A;t)=\sum_n nP_n(t)=6 \tag{7}$$

(Euler's theorem). We choose to neglect neighbor correlations in our description of these vanishing processes. We have three motivations to do so.

(1) We wish to write down a *minimal* model—the simplest possible model yielding realistic results—as an analytic device for studying the relative importance of various features of froths. Surely, whatever features we leave out of the model cannot contribute to results, while it is impossible to gauge the relative importance of features included. We do not see this minimal model as a final model, but rather as a starting point to which more features may be added for realism, once the minimal version is understood. That is not done in the present article, however.

(2) Surely, a minimal model will more willingly yield results than a more complex one. From many different contexts it is well known that the neglect of correlations is a crucial step towards a solvable model. Here too. As shown in Appendix B, this step renders the model "almost solvable" by analytical means. A popular hypothesis for a certain distribution function is falsified; a number of analytical results are obtained below.

(3) Correlations are weak according to Aboav-Weaire's law, suggesting that we may neglect them entirely without seriously compromising results.

Neglecting correlations, we assume that any bubble is the neighbor of any other bubble with a probability proportional to its number of edges, or neighbors. Specifically, we assume that any bubble is an *affected* neighbor of any *vanishing* bubble with a probability proportional to the number of edges of the first bubble. With this assumption, we have also given a specific answer to a difficult open key question in the formulation of any theory for coarsening froths: when a four- or five-sided bubble vanishes from a froth, which of its neighbors have their topologies changed? See [32, 1] and compare with [12]. Because of this assumption we call the model a "random-neighbor model" [45]. Our random-neighbor relationship is "annealed," not "quenched," meaning it is rechosen, whenever it is used. Consequently, the only geometrical relationships respected by this model are Euler's theorem and those embodied in von Neumann's law.

Thus we arrive at a transition rate $T_{n,m}(t)$ from topology m to n of the form

$$T_{n,m}=\begin{cases}c_+(n-1) & \text{for}\quad m=n-1\\ \dot{\bar{A}}/\bar{A}-(c_++c_-)n & \text{for}\quad m=n\\ c_-(n+1) & \text{for}\quad m=n+1\\ 0 & \text{for}\quad m\neq n-1,n,n+1\end{cases} \tag{8}$$

with

$$c_+=\tfrac{1}{6}|v_5|\,p_5(0;t), \tag{9}$$

$$c_-=\tfrac{1}{6}\sum_{k=0}^{5}(k-6)\,v_k\,p_k(0;t)+c_+,$$

$$\dot{\bar{A}}/\bar{A}=\sum_{k=0}^{5}|v_k|\,p_k(0;t). \tag{10}$$

Here $6c_+$ and $6c_-$ are the rates at which topological numbers are incremented and decremented, respectively, by the vanishing processes in Fig. 2(a). We simply neglect the neighbor switching process shown in Fig. 2(b). We have two motivations for this: our desire to define a minimal model and experimental indications discussed in Sec. XI. This leaves us with a model containing no adjustable parameters at all. All rates are determined dynamically.

Our final result for the master equation is

$$\left(\frac{\partial}{\partial t}+v_n\frac{\partial}{\partial A}\right)p_n(A;t)=\sum_{m=n-1}^{n+1}T_{n,m}\,p_m(A;t)$$

$$\text{for}\quad n=0,1,2,\ldots. \tag{11}$$

This first-order partial-differential equation is neither linear nor local, since $p_m(A;t)$ is multiplied by $T_{n,m}$ which contains $p_k(0;t), k=0,1,2,\ldots,5$. One can easily show, though, that Eq. (11) makes the obvious relation

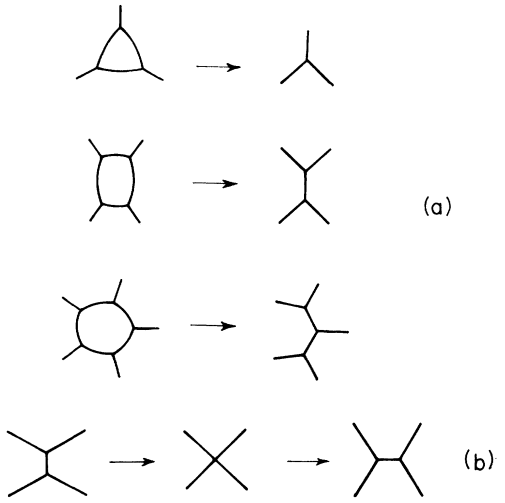

FIG. 2. (a) Vanishing of domains with 3, 4, and 5 neighbors, so-called $T2$ processes. (b) Neighbor switching, so-called $T1$ process.

$$\bar{A} = \sum_{n=0}^{\infty} \int_0^{\infty} dA\, A\, p_n(A;t), \tag{12}$$

consistent with Eq. (10) when Eq. (7) is satisfied.

Equation (11) is almost identical to the "gas approximation" by Fradkov, Udler, and Kris [46] with a crucial difference: We insist on having no neighbor correlations in the model, and are consequently forced to accept the presence of bubbles with 0 and 1 edges, in addition to those with 2,3,4,... occurring in [46]. We are forced the following way: in the random choice of neighbors to a vanishing bubble, bubbles with topology n are chosen with probability proportional to n to become bubbles with topology $n-1$. Consequently, the dynamics forces all non-negative topologies into the ensemble. As we shall see, our model assigns negligible probability to bubbles with 1 and 0 edges. So though they are mathematical artifacts, we accept their presence in order to be consistent with the random-neighbor approximation. As a fringe benefit, this also keeps the model mathematically simple, to an extent that makes it possible to obtain several results analytically. Actually, our model is so simple that it is almost solvable when a simple assumption is made; see Appendix B. Another difference to the model in [46] is our dynamical definition of c_+ above. In [46], c_+ describes all topology-incrementing processes, i.e., both T_1 and T_2 processes, and is not determined dynamically, but by fitting to experimental data. We could do that, too, but we find a parameter-free theory more challenging since its case can be argued, as we have done.

Equation (11) also resembles a theory by Marder [47], but our expression for $T_{n,m}$ is much simpler. It also resembles a mean-field theory by Beenakker [48], with the crucial difference that Beenakker makes a specific ansatz for the shape and topology n of a bubble with a given area A. Finally one may compare our model with the simulations of Fradkov and Udler and Beenakker, described in [49] and [50], respectively. They also approximate a froth by an ensemble of individual bubbles obeying von Neumann's law and Euler's theorem, but keep track of neighbor relations. Where our model is annealed, their models are quenched. Consequently, they have no master equation expressible in terms of single-bubble distributions. All the mentioned models resemble each other, because they all embody von Neumann's law and Euler's theorem. They differ only in their treatment of neighbor relations in topology changing processes. Apparently small differences in that treatment have profound consequences for the models' tractability, dynamics, and predictions, however.

IV. SCALE-INVARIANT EQUATIONS, NORMAL GROWTH

Our master equation (11) contains only one independent, dimensionfull parameter, v_7 for example. We absorb a factor v_7 in t. Then t has dimension area, and the rates in Eq. (1) become dimensionless integers: $v_n = n-6$. Introducing the relative area

$$x = A/\bar{A}(t), \tag{13}$$

and dimensionless functions

$$f_n(x;t) = \bar{A}(t)\, p_n(A;t), \tag{14}$$

we have

$$P_n(t) = \int_0^{\infty} dx\, f_n(x;t), \tag{15}$$

and the master equation (11) takes the form

$$\begin{aligned} \bar{A}\frac{\partial}{\partial t} f_n(x;t) = &\left[[-(n-6) + \dot{\bar{A}}x]\frac{\partial}{\partial x} + 2\dot{\bar{A}} \right. \\ &\left. -(c_+ + c_-)n \right] f_n(x;t) \\ &+c_+(n-1) f_{n-1}(x;t) \\ &+c_-(n+1) f_{n+1}(x;t). \end{aligned} \tag{16}$$

Here c_+ and c_- have been redefined by absorbing a factor $\bar{A}/v_7$ into them, so that now they are dimensionless,

$$c_+ = \tfrac{1}{6} f_5(0;t), \quad c_- = \tfrac{1}{6} \sum_{k=0}^{5} (k-6)^2 f_k(0;t) + c_+. \tag{17}$$

So $\dot{\bar{A}}$ is now

$$\dot{\bar{A}} = \sum_{k=0}^{5} (6-k) f_k(0;t). \tag{18}$$

Finally we need

$$\bar{A}(t) = \int_0^t dt' \dot{\bar{A}}(t') \tag{19}$$

to have a closed set of equations. In a numerical integration of Eq. (16) it is more convenient to work with a scale-invariant, dimensionless "time" parameter

$$\tau = \int_0^t \frac{dt'}{\bar{A}(t')} \tag{20}$$

since $\bar{A}\frac{\partial}{\partial t} = \frac{\partial}{\partial \tau}$.

The norm and the two first moments of the dimensionless distributions $f_n(x;t)$ are conserved as a consequence of Eqs. (6), (7), and (13),

$$\mu_0 = \sum_{n=0}^{\infty} \int_0^{\infty} dx\, f_n(x;t) = \sum_{n=0}^{\infty} P_n(t) = \int_0^{\infty} dx f(x) = 1, \tag{21}$$

$$\mu_1 = \sum_{n=0}^{\infty} \int_0^{\infty} dx\, n f_n(x;t) = \sum_{n=0}^{\infty} n P_n(t) = 6, \tag{22}$$

$$\langle x \rangle = \sum_{n=0}^{\infty} \int_0^{\infty} dx\, x f_n(x;t) = \int_0^{\infty} dx\, x f(x;t) = 1. \tag{23}$$

In these equations we have used the definition

$$f(x;t) = \sum_{n=0}^{\infty} f_n(x;t) \tag{24}$$

for the frequency of bubbles with relative area x and any topology. In Sec. VIII we detail how these conservation laws are satisfied by Eq. (16).

Equations (16)–(19) are the fundamental equations of our theory. The coupled, nonlinear and nonlocal partial-differential equations (16) describe transport of probability and dilation along the x axis, and transport and diffusion along the n axis. The transport in the x variable is just von Neumann's law, while the dilation term $\dot{\bar{A}} x \frac{\partial}{\partial x}$ reflects the time dependence of the unit $\bar{A}$ in which x measures areas. The terms containing c_+ and c_- can be written as a sum of a transport term and a diffusion term for the probability distribution for topology, $n/6 f_n(x;t)$,

$$\begin{aligned} &-(c_+ + c_-) n f_n + c_+(n-1) f_{n-1} + c_-(n+1) f_{n+1} \\ &\quad = \tfrac{1}{2}(c_- - c_+)[(n+1) f_{n+1} - (n-1) f_{n-1}] \\ &\qquad + \tfrac{1}{2}(c_+ + c_-)[(n+1) f_{n+1} - 2n f_n \\ &\qquad + (n-1) f_{n-1}]. \end{aligned} \tag{25}$$

Here the first term on the right-hand side describes a flow of probability along the n axis with velocity $-6(c_- - c_+)$. The second term describes diffusion of probability along the n axis with diffusion constant $3(c_+ + c_-)$. This diffusion term is the only dispersive term in the equations. It is responsible for their having a unique attractive fixed point for their development in time, in the form of a stationary solution $f_n(x)$. The corresponding value for $\dot{\bar{A}}$ is obviously also stationary, and consequently $\bar{A} = \dot{\bar{A}} t$ at the fixed point. This scaling law is usually expressed in terms of a characteristic length-scale, which consequently is proportional to $t^{1/2}$. The exponent $1/2$ is called the growth exponent. Its value is a consequence of von Neumann's law.

At the attractive fixed point, the froth's coarsening process is self-similar, since all distributions $f_n(x)$ for relative areas are constant; the only time-dependent quantity is the overall scale set by $\bar{A}(t)$. This is called *normal growth*. Normal growth was established experimentally for 2D soap froths by Smith [51] and, independently, by Fullman [52] in 1952. Almost 30 years later, Aboav analyzed a different set of Smith's original data, and found μ_2, the second moment of P_n, increasing linearly with time [42]. This absence of normal growth instigated much creativity until Glazier, Gross, and Stavans demonstrated experimentally that Aboav's finding for μ_2 was transient behavior [38]. Normal growth was only recently rigorously reestablished experimentally by Stavans and Glazier [1], Stavans [3], and Glazier, Anderson, and Grest [11]. In simulations representing the 2D froth by a Potts model, normal growth was established in [53, 54]. In direct simulations of froths, the second topological moment μ_2 has been shown to be time independent asymptotically, but with some disagreement over its value [16, 25]. Herdtle and Aref have rather convincingly demonstrated that the topological distribution P_n is constant asymptotically in time, and independent of initial conditions, in their direct simulations [25]. The vertex models studied by Kawasaki and co-workers are computationally more efficient than the ideal froth, and normal growth with exponent $1/2$ has been established for these models, even though they do not obey von Neumann's law [22].

In general, these demonstrations of normal growth are difficult because it is pursued as an asymptotic property of the system's dynamics for $t \to \infty$. Not that there is any other way to do this. But since one always has to start experiments and simulations with a finite sample, and bubbles disappear as asymptotia is approached, the closer the approach is, the poorer are the statistics.

V. NUMERICAL SOLUTION

The master equation (16) was integrated numerically to $t = \infty$, effectively, to find its fixed-point solution $f_n(x)$ as $\lim_{t\to\infty} f_n(x;t)$. This was not an entirely trivial task. From the *physical* point of view, the fixed point is attractive, and by integrating Eq. (16) forward in time we should end up at this fixed point irrespective of our choice of initial state, as long as this state does not belong to the set of repulsive fixed points

$$f_n(x) = \delta_{n,6} f(x), \tag{26}$$

where $f(x)$ is an arbitrary, non-negative function of $x \geq 0$ satisfying Eqs. (21) and (23). From the *numerical* point of view, however, the fixed point is hyperbolic: any violation of the conservation laws (21) and (22) by discretization errors, round-off errors, or finite-size errors, will grow exponentially in time, and entrain exponentially growing violations of Eq. (23). We used $f_n(x_i;\tau_j)$ with $x_i = i\Delta x$ and $\tau_j = j\Delta\tau$ as numerical variables, and wrote an algorithm for these variables which conserves their normal-

ization and two first moments exactly, without any discretization errors. The algorithm was implicit to assure numerical stability, and was solved by Gauss elimination with back substitution. We found finite-size effects negligible at the fixed point, when the necessary cutoffs in x and n were chosen as $x_{\max} = 25$ and $n_{\max} = 30$. We set $f_n(x;t) = 0$ beyond these cutoffs, and used open boundary conditions, i.e., probability could flow out of the system across the cutoffs, but no probability could flow into the system, since $f_n(x)$ vanished beyond the cutoffs. With these cutoffs, $P_{n_{\max}} \simeq 10^{-14}$ and $f(x_{\max}) \simeq 10^{-17}$, so the rate at which the conservation laws (21), (22), and (23) were violated by loss of probability at the cutoffs was negligible compared to the rate at which round-off errors were introduced.

The values for μ_0, $\mu_1/6$, and $\langle x \rangle$ were monitored, and whenever they differed from 1 by more than 0.5×10^{-4}, $f_n(x)$ was mapped back into the physical subset of distributions, and thereby onto a trajectory flowing into the fixed point. This was done by multiplying it by $\alpha \exp(-\beta x - \gamma n)$, and choosing α, β, and γ such that $\mu_0 = 1$, $\mu_1 = 6$, and $\langle x \rangle = 1$. Since the fixed point is unique, and attractive in the physical degrees of freedom, the fixed-point result for $f_n(x)$ is independent of how we get there. But it is, of course, not possible to give the *time evolution* of $f_n(x;t)$ with this method.

Evidently, it is crucial to the success of our algorithm that its makes $f_n(x;\tau)$'s physical component flow faster towards the fixed point than it makes its unphysical component flow out of it. This is why the algorithm was engineered to conserve μ_0, μ_1, and $\langle x \rangle$ without discretization errors. With only round-off errors and negligible finite-size errors contributing to the unphysical components, this inequality between flows was amply fulfilled. Yet the mapping back to physical distributions had to be applied regularly.

As the initial state we used

$$\begin{aligned} f_n(x;0) &= P_n(0) f(x;0), \\ P_n(0) &= 1/7(6/7)^n, \\ f(x;0) &= \exp(-x) \end{aligned} \tag{27}$$

with larger cutoffs than those mentioned above, but also the rather large value 0.8 for Δx. This large value for Δx permitted use of a rather large value for $\Delta\tau$. After a computationally fast convergence to the fixed point on this coarse lattice, the cutoffs were lowered, since the solution showed this was possible, Δx and $\Delta\tau$ were halved, and the integration continued on the finer lattice from the state obtained on the coarser lattice (interpolated, where necessary, to define its values on the finer lattice). This procedure of solving, halving Δx, adjusting $\Delta\tau$, and solving again, was repeated several times. In the end, converged results for each lattice were used to extrapolate to the continuum limit, $\Delta x = 0$. This procedure much reduced the computational task of approaching the fixed point. This was necessary, because this approach is inherently slow on physical grounds. As we mentioned in Sec. IV, the master equation (16) is dissipative only along the n axis. The dissipation of probability along the x axis, which is necessary to make $f_n(x;t)$ converge to its fixed-point form, comes about only by dissipation along the n axis, combined with transport along the x axis with velocities depending on n. This is why the convergence to the fixed point is slow.

VI. THE DISTRIBUTIONS $f_n(x)$

Our fixed-point result for the functions $f_n(x)$ are shown in Fig. 3. Table I lists our results for $f_n(0)$, P_n (see Sec. VII), and $\langle x \rangle_n$ (see Sec. IX). Table II gives $\breve{A}$, c_+, and c_-, and Table III gives the moments of P_n (see Sec. VIII).

The distributions $f_n(x)$ are traditionally displayed as in Fig. 4(a), which shows $x f_n(x)/\log_{10}(e)$ against $\log_{10}(x)$ as fully drawn curves. The graph with the highest maximum corresponds to $n = 6$. Peaking to the right of it are curves corresponding to $n = 7$, 8, 9, 10, and, barely visible, 11. Peaking to the left of it are curves corresponding to $n = 5$, 4, and, barely visible, 3. The areas under the curves are P_n, the frequency of bubbles with topology n and any area. The dashed curve shown is the graph of $x f(x)/\log_{10}(e)$, i.e., the frequency of bubbles with relative area x and any topology. The dotted curve shown is $x \exp(x)/\log_{10}(e)$, the distribution for x which is obtained when the master equation (16), and the physics embodied in it, is ignored, and the entropy of $f(x)$ is maximized under the constraints given in Eqs. (21) and (23).

The results in Fig. 4(a) may be compared with those in Fig. 4(b), obtained in a Monte Carlo simulation that represents the froth by a Potts model on a triangular lattice, quenched from infinite to zero temperature [[53],Fig. 21]. Notice the trivial factor 10 between the quantities plot-

TABLE I. $f_n(0)$, P_n, and $\langle x \rangle_n$ at the attractive fixed point of the scale invariant master equation (16).

n	$f_n(0)$	P_n	$\langle x \rangle_n$
0	0.262×10^{-5}	0.793×10^{-6}	0.300
1	0.146×10^{-3}	0.471×10^{-4}	0.317
2	0.319×10^{-2}	0.111×10^{-2}	0.341
3	0.340×10^{-1}	0.132×10^{-1}	0.375
4	0.179	0.827×10^{-1}	0.430
5	0.416	0.258	0.535
6	0.270	0.347	0.777
7	0	0.184	1.42
8	0	0.747×10^{-1}	2.16
9	0	0.266×10^{-1}	2.94
10	0	0.870×10^{-2}	3.76
11	0	0.267×10^{-2}	4.59
12	0	0.787×10^{-3}	5.43
13	0	0.224×10^{-3}	6.27
14	0	0.622×10^{-4}	7.13
15	0	0.169×10^{-4}	7.99
16	0	0.450×10^{-5}	8.85
17	0	0.118×10^{-5}	9.71
18	0	0.305×10^{-6}	10.6
19	0	0.780×10^{-7}	11.4
20	0	0.198×10^{-7}	12.3

TABLE II. $\bar{A}$, c_+, and c_- as determined from $f_n(0)$ in Table I.

$\bar{A}$	c_+	c_-
0.890	0.0693	0.318

ted in Figs. 4(a) and 4(b). The two sets of results are seen to agree both qualitatively and, to quite an extent, also quantitatively. The "wiggles" in the curves shown in Fig. 4(b) are due to counting and binning problems caused by limited statistics.

Log-normal distributions have been used with some success to describe distributions like those shown in Fig. 4(b), but obtained from 2D sections of 3D polycrystals [55]. Clearly, the distributions obtained here and shown in Fig. 4(a) come closer to those in Fig. 4(b) than any log-normal distributions possibly can, because they are symmetric about the positions of their maxima. In addition to this phenomenological advantage, our distributions are also the result of a theory, and involve no fitting.

Figure 5(a) shows $f_n(x)/P_n$ against x for $n = 5$, 6, 7, and 8. The curve with maximum at $x = 0$ corresponds to $n = 5$. As n increases, the x coordinate of the maximum increases, and the maximum value decreases. One may convince oneself, using Eq. (16), that $f_n(x) \sim x^{n-6}$ for $x \sim 0$ for $n \geq 6$. This is also seen in Fig. 5(a). These curves should be compared with those in Fig. 5(b), which are experimental results for 2D soap froths (full curves) and simulation results for a Potts model on a triangular lattice (dashed curve) ([11],Fig. 19). These figures, too, are seen to agree both qualitatively and to some extent quantitatively. It would be very nice to have less noisy experimental and simulation results to compare with.

Figure 6 shows $f_n(x)$ against x plotted with a logarithmic second axis in order to make visible the graphs corresponding to small and large values for n. One sees that $f_n(x)$ decreases exponentially for x large. The graph just visible in the lower left corner of the figure is that of $f_0(x)$. The decreasing graph immediately above it is that of $f_1(x)$, etc. up to $f_{16}(x)$ just visible in the lower right corner of the figure. The smooth and regular nature of the curves invites speculations whether simple analytical expressions for them exist. After all, Eq. (16) contains only integers—with 6 having a special status—and the constants $\bar{A}$, c_+, and c_- themselves determined from Eq. (16). Since Eq. (16) maximizes the entropy, the exponential function occurs naturally. But since the integer 6 replaces 2π in our kind of two-dimensional geometry, not even π may occur naturally. Unfortunately, we know no such simple expressions for $f_n(x)$, but Appendix B gives an impression of what they might look like. Here we only remark that the functions $f_n(x)$ shown in Fig. 6 seem to decrease as $\exp(-3x)$ for $x \geq n$.

Figure 7 shows yet another way to present the distributions $f_n(x)$: The curves shown are $\sum_{n'=0}^{n} f_{n'}(x)/f(x)$, starting with the curve for $n = 3$ in the lower left corner

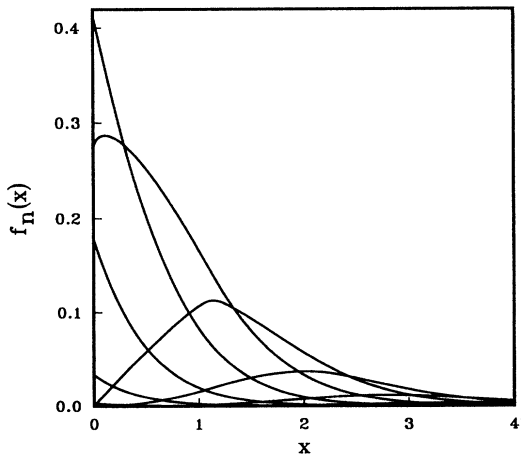

FIG. 3. Distributions $f_n(x)$ vs x, starting with $n = 3$ in the lower left corner. Distributions having $n = 0$, 1, and 2 are too small to show in this plot. For $n \geq 6$ and $x \sim 0$, $f_n(x) \sim x^{n-6}$.

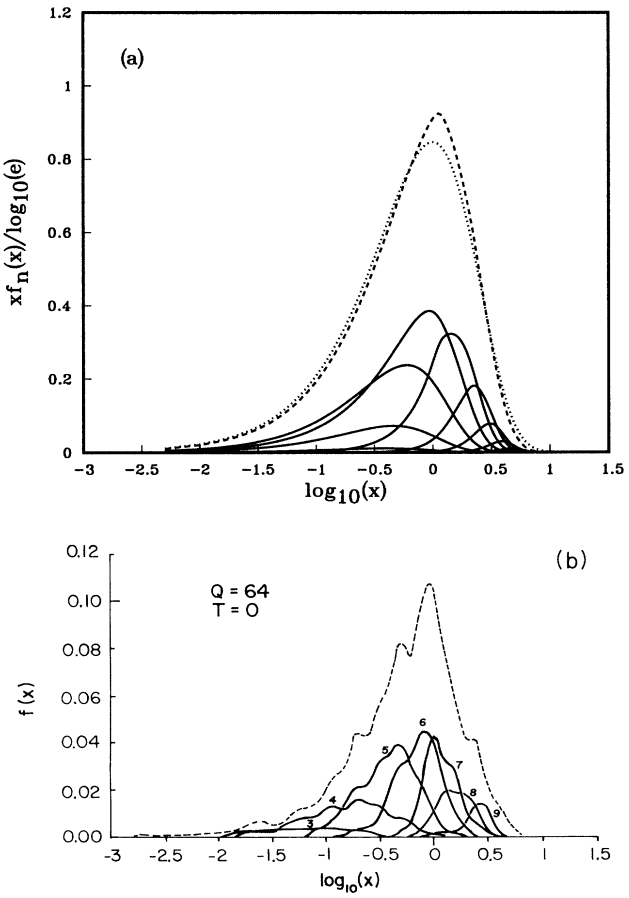

FIG. 4. (a) Fully drawn curves: distributions $xf_n(x)/\log_{10}(e)$ vs $\log_{10}(x)$. Dashed curve: their sum $xf(x)/\log_{10}(e)$ vs $\log_{10}(x)$. Dotted curve: distribution $x\exp(x)/\log_{10}(e)$ vs $\log_{10}(x)$. (b) Potts model simulation results for $0.1xf_n(x)/\log_{10}(e)$ vs $\log_{10}(x)$ (fully drawn curves), and their sum $0.1xf(x)/\log_{10}(e)$ (dashed curve); from [53].

TABLE III. Moments and width of topological distribution P_n as obtained with the random-neighbor model (RNM) and in experiments [11].

Source	μ_0	μ_1	μ_2	μ_3	μ_4	w
RNM	1	6	1.70	1.34	12.4	0.936
Experiment	1	5.933	1.486	1.105	7.154	0.940

of the figure and ending with the curve corresponding to $n = 17$ just visible in the upper right corner. The vertical distance between the $(n-1)$th curve and the nth curve is $f_n(x)/f(x)$. So the figure shows the partitioning of 1 into $f_n(x)/f(x)$ for $0 \le x \le 10$. Beenakker's mean-field theory in [48] replaces the curves in Fig. 7 with vertical lines at specified x coordinates. It is rather obvious from Fig. 7 that $\langle n \rangle_x$ approximately is a first-degree polynomial in x.

VII. THE DISTRIBUTION OF TOPOLOGY P_n

We obtain an equation for P_n by integrating both sides of Eq. (16) with respect to x,

$$\bar{A}\frac{d}{dt}P_n = \Theta_{6-n}(n-6)f_n(0;t) + \dot{\bar{A}}P_n - (c_+ + c_-)nP_n + c_+(n-1)P_{n-1} + c_-(n+1)P_{n+1}, \tag{28}$$

where Θ is Heaviside's function

$$\Theta_k = \begin{cases} 1 & \text{for} \quad k > 0 \\ 0 & \text{for} \quad k < 0. \end{cases} \tag{29}$$

Since Stavans, Domany, and Mukamel recently have suggested a somewhat similar equation [28], we compare the two equations in some detail: In [28], the notation x_ℓ is used, where we use P_n. To avoid confusion, we maintain our own notation. There are three differences between our Eq. (28) and theirs.

(1) We choose any bubble as neighbor to a vanishing bubble with a probability proportional to the number of sides possessed by the chosen bubble and the frequency with which its topology occurs. This gives the explicit factors n and $n \pm 1$ in the last three terms in Eq. (28), and the factors P_n and $P_{n\pm1}$ they multiply. In [28], neighbor bubbles are also chosen at random, but simply with the frequency P_n with which they occur.

(2) In [28], bubbles with zero, one, and two neighbors are excluded from the theory. The terms assuring this introduce nearest-neighbor correlations, and give a higher-order equation in P_n than ours. We permit bubbles with zero, one, and two neighbors as a mathematical artifact, forced upon us by our insistence on a theory without correlations. Simpler equations result.

(3) In [28], the equation corresponding to Eq. (28) contains three unknown functions, the equivalents of $f_3(0;t)$, $f_4(0;t)$, and $f_5(0;t)$. Their values at $t = \infty$ are treated

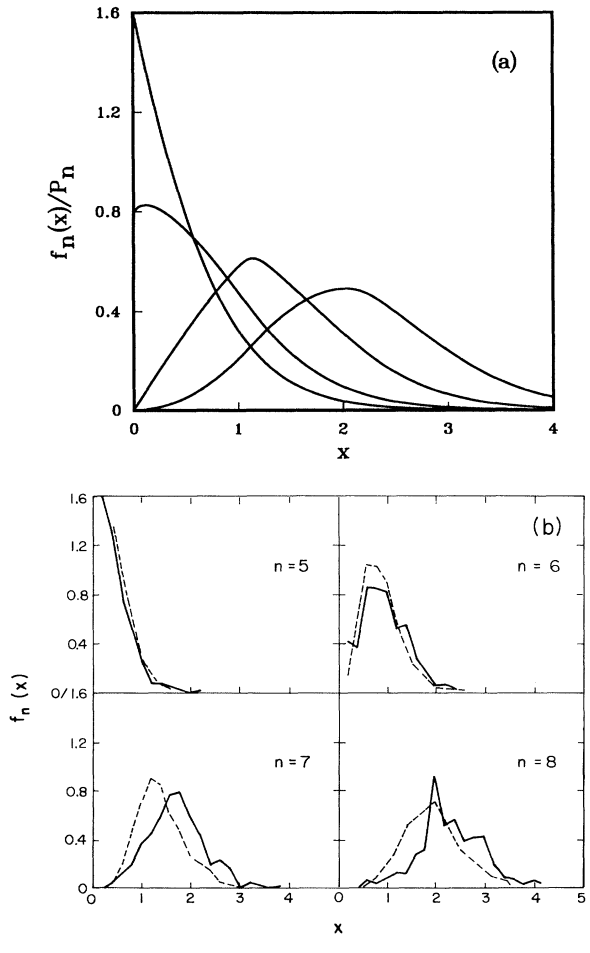

FIG. 5. (a) $f_n(x)/P_n$ vs x for $n = 5$, 6, 7, and 8. (b) The same functions from 2D soap froth experiment (fully drawn curves) and Potts model simulation (dashed curves) [11] .

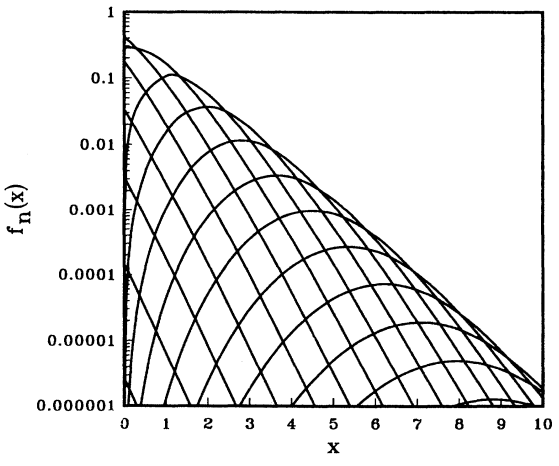

FIG. 6. $f_n(x)$ vs x with logarithmic second axis.

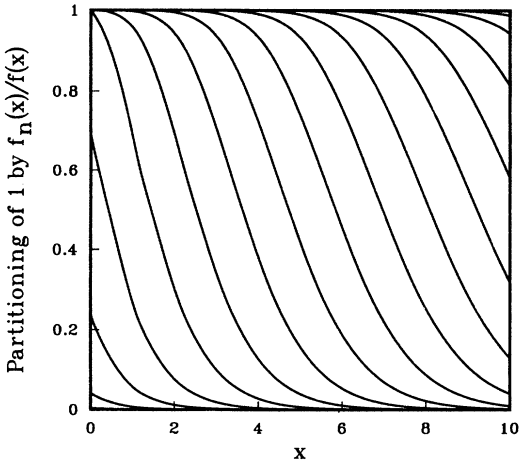

FIG. 7. The partitioning of 1 by $f_n(x)/f(x)$ for $x \in [0, 10]$. The curves shown are $\sum_{n'=0}^{n} f_{n'}(x)/f(x)$ vs x, starting with $n = 3$ in the lower left corner of the plot.

as free parameters and used to fit P_n to experimental results. We have $f_n(x;t)$, not $P_n(t)$, as a fundamental variable, and thereby obtain a closed set of equations, the master equation (16). This set of equations uniquely determines $f(x;\infty)$, and $f(0;\infty)$ with it, independent of initial data. Our $P_n(\infty)$ is just the integral of $f_n(x;\infty)$, with no parameters to be fitted.

At the fixed point, the left-hand side of Eq. (28) vanishes, and we can find P_n's asymptotic dependence on n. Assuming $P_n \sim \lambda^n$, we find

$$0 = -(c_+ + c_-)\lambda + c_+\lambda^{-1} + c_-\lambda, \tag{30}$$

which is solved by $\lambda = 1$ and by $\lambda = c_+/c_-$. So P_n can be any linear combination of 1 and $(c_+/c_-)^n$, with $P_n \sim (c_+/c_-)^n$ obviously being the only normalizable solution. We have also found the first two correction terms to this result in a systematic expansion in $1/n$, and have

$$P_n \propto (c_+/c_-)^n n^{[\dot{A}/(c_- - c_+)]-1}[1 + a_1/n + O(1/n^2)], \tag{31}$$

$$a_1 = \frac{-\dot{A}(\dot{A} - c_- + c_+)(c_- + c_+)}{2(c_- - c_+)^3}. \tag{32}$$

Figure 8(a) shows our result for $\log_{10}(P_n)$. The exponential decrease at large values of n shows clearly. So does the relative unimportance of P_n for $n = 0$, 1, and 2. The numerical values for P_n are given in Table I.

Figure 8(b) shows our result for P_n as filled circles, and the experimental values given in [11] as diamonds with error bars. The two sets of results are seen to agree, albeit with some discrepancy for $n = 5$ and 6, where the experimental error bars are smallest. A comparison of our values for P_n with the experimental values gives $\chi^2 = 14.3$. There are nine degrees of freedom in the 11 data points we compare with, because they satisfy the linear constraints $\mu_0 = 1$ and $\mu_1 = 6$. Consequently, we have 12% χ^2 backing for the hypothesis that the data are described by our results. We believe that the discrepancies at $n = 5$ and 6 are significant. They may not signal a shortcoming of our model, however, but rather a difference between the experimental froths and the ideal, dry, 2D froth we model: while it is experimentally well established that $P_5 > P_6$ both for foams and for low anisotropy metals, Herdtle and Aref report $P_6 > P_5$ by a factor 1.2 from their extensive simulations of ideal, dry froths in 2D [25]. Clearly, we should compare our result with theirs rather than with experimental results, when the two types of results differ, since it is the ideal, dry 2D froth we model. Unfortunately, Herdtle and Aref do not report their numerical values for P_n apart from $P_6 = 0.35$—to be compared with our value $P_6 = 0.347$—so a closer comparison is not possible. We can only compare our value for P_6/P_5, 1.34, with their value 1.2. Comparing again with experimental values for 2D soap froth listed in [[11],Table I] and [[35],Table VII], we notice that our values for P_n come closer than any of the mean-field results listed in [[11],Table I] and [[35],Table VII]. Our results for P_n's moments are discussed in the next section.

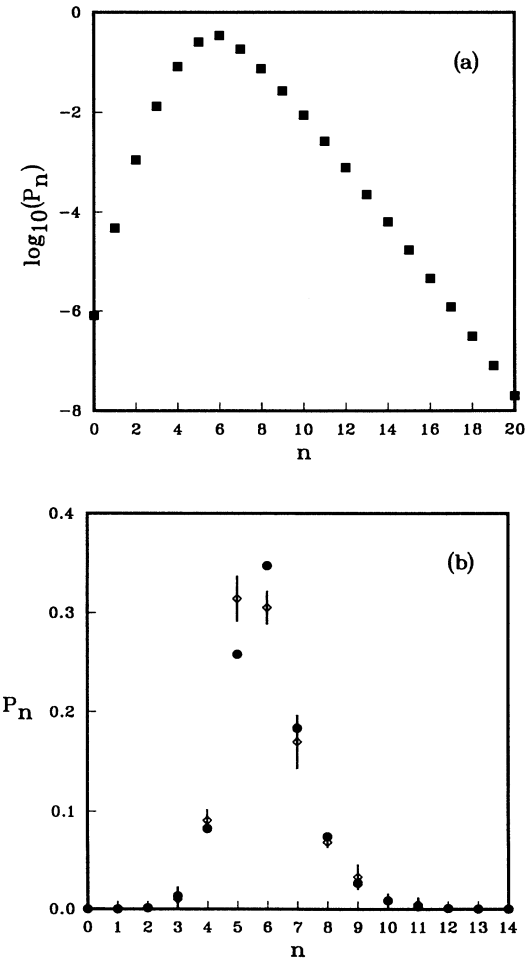

FIG. 8. (a) $\log_{10}(P_n)$ vs n. (b) P_n vs n. Filled circles show results of the random-neighbor model. Diamonds with error bars are results from 2D soap froth experiments [11].

VIII. MOMENTS

By summing Eq. (28) over n, we find

$$\bar{A}\frac{d}{dt}\mu_0 = \dot{\bar{A}}(\mu_0 - 1). \tag{33}$$

This equation tells us two things. First, the total probability μ_0 is conserved in time, as it should be, by our model, provided it is 1 from the start. Second, the value 1 is a repulsive fixed point for the dynamics; so any discretization or round-off error in a numerical attempt to solve Eq. (16) will grow exponentially with time. Put another way: the attractive fixed point for the Markov process described by Eq. (16) is elliptic only for the physical degrees of freedom. Viewed as a numerical problem, other degrees of freedom are invoked, and the fixed point sought is hyperbolic.

The situation is the same for the other two conserved moments: By multiplying both sides of Eq. (28) with n, and summing over n, we find

$$\bar{A}\frac{d}{dt}\mu_1 = (\dot{\bar{A}} - c_- + c_+)(\mu_1 - 6). \tag{34}$$

It is easy to prove that $\dot{\bar{A}} > c_- - c_+$, so Eq. (34) shows that Euler's theorem, $\mu_1 = 6$, is conserved in time, if it is satisfied from the start, but also that it is a repulsive fixed point for the dynamics. Similarly, we find for $\langle x\rangle$:

$$\bar{A}\frac{d}{dt}\langle x\rangle = \mu_1 - 6\mu_0, \tag{35}$$

which shows that even if initially $\langle x\rangle = 1$, as it should be, it does not remain at this value, if $\mu_1/\mu_0 = 6$ is violated for example by round-off errors in a numerical integration of Eq. (16).

The moments μ_m beyond the first two do not have fixed values, and their equations derived from Eq. (16) contain some information about the fixed-point solution to Eq. (16). For example, the second moment obeys

$$\bar{A}\frac{d}{dt}\mu_2 = -\sum_{n=0}^{5}(6-n)^3 f_n(0;t) + 6(c_+ + c_-) + [\dot{\bar{A}} - 2(c_- - c_+)]\mu_2. \tag{36}$$

At the fixed point, the right-hand side of this equation vanishes, and we have

$$\mu_2 = \frac{\sum_{n=0}^{5}(6-n)^3 f_n(0) - 6(c_+ + c_-)}{\dot{\bar{A}} - 2(c_- - c_+)}. \tag{37}$$

For $\mu_2 > 0$, the numerator and denominator in this expression must have the same sign. This gives two inequalities between the values of $f_n(0;\infty), n = 0,\ldots,5$. Similar equations of increasing complexity may be derived for higher moments. These fixed-point equations must not be read as relations between more or less free parameters, however. They are direct consequences of our master equation which *also* determines the values of $\dot{\bar{A}}$, c_+, c_-, and $f_n(0)$, $n = 0,1,\ldots,5$ at its unique fixed point. The time dependence of μ_2 expressed in (36), however, may be used to explain the nonmonotonic approach of μ_2 to its asymptotic fixed-point value observed for an initially ordered froth in [[1], Fig. 1], [[11], Fig. 9], and [[16], Fig. 1]. Using the definitions (17) and (18), we write out (36) as

$$\begin{aligned}\bar{A}\frac{d}{dt}\mu_2 = {} & \tfrac{2}{3}(3+\mu_2)f_5(0;t) - \tfrac{2}{3}(6-\mu_2)f_4(0;t) \\ & -18f_3(0;t) - \tfrac{4}{3}(36+\mu_2)f_2(0;t) \\ & -\tfrac{10}{3}(30+\mu_2)f_1(0;t) - 6(30+\mu_2)f_0(0;t).\end{aligned} \tag{38}$$

In an ordered froth consisting mainly of six-sided bubbles with a low density of five- and seven-sided bubbles, μ_2 is small—actually equal to $P_5 + P_7 = 2P_5$—and the right-hand side of (38) contains only non-negative terms. To the extent five-sided bubbles vanish, $f_5(0;t) > 0$ and μ_2 grows exponentially plus linearly with time. The vanishing of five-sided bubbles creates more five-sided bubbles from the predominant six-sided ones, and some four-sided bubbles from five-sided ones. Both creation processes increase μ_2's value by increasing P_5 and P_4, while it is only later, when the four-sided bubbles have shrunk to vanish, that the second term on the right-hand-side of (38) turns negative from zero. It takes even more time before three-sided bubbles are created from four-sided ones and the third term on the right-hand side turns negative from zero, and so forth for the fourth, fifth, and sixth terms. The key point then is as follows: (38) shows that it is only the *vanishing* of bubbles with four or fewer sides that will decrease μ_2, and only if it happens at a sufficient rate compared to the vanishing of five-sided bubbles. But before four- and fewer-sided bubbles can vanish at a sufficient rate, they must be created. And their creation *increases* μ_2. Consequently, μ_2 must first increase and keep increasing, overshooting its equilibrium value, because only through this increase and with a delay—the time it takes few-sided bubbles to shrink to zero area—can those processes get started which will make $d\mu_2/dt$ decrease and vanish.

Our numerical results for P_n's width

$$w = \sum_{n=0}^{\infty}|n-6|P_n \tag{39}$$

and moments at the fixed point are shown in Table III, together with experimental values for 2D froths from [11]. Our value for the second moment may also be compared with the values obtained in direct simulations of the ideal, dry, 2D froth. This is a more relevant comparison when the quality of our two approximations is the issue, since the contribution of nonideal effects in experimental results is unknown. Unfortunately there is no agreement between simulation results: $\mu_2 = 1.42 \pm 0.05$ according to [16], while $\mu_2 = 1.2$ according to [25] with no error bars given. The error bars are significantly smaller than the discrepancy of 0.2, however, judging from Fig. 10 in [25]. See [25] for a discussion of this discrepancy. It would be nice and useful if the precision of direct simulations could be pushed to a level where higher moments could also be

given.

Our too large value for μ_2 would presumably be reduced if we took into account that nearest neighbors to vanishing bubbles have topologies which, on the average, are larger than those obtained with our random choice, according to Aboav-Weaire's law. Yet, as they stand, our results for the moments of P_n are much closer to the experimental values than any of the mean-field results listed in [[11],Table II].

Another experimentally accessible moment is $f(x)$'s second, $\langle x^2\rangle - 1$, for which we find the value 0.858 numerically. It may be compared with the value 1 obtained for $f(x) = \exp(-x)$—a form for $f(x)$ discussed in Sec. X and Appendix B—and with the value 0.5 found in experiments with froth patterns in monolayers [8].

IX. LEWIS'S LAW

Lewis discovered that a simple linear relationship is obeyed by cell structures in cucumber skin, human amnion, and pigmented epithelium of the retina [56]. With our notation, and in terms of scale invariant, dimensionless variables, it reads

$$\langle x\rangle_n = \alpha(n-6)+1 \qquad \text{(Lewis's law)}. \tag{40}$$

Most undifferentiated biological tissues seem to obey this phenomenological law, though the evidence is not conclusive [57, 13]. Rivier and Lissowski have derived it very elegantly by a simple maximum entropy argument applied to the topological distribution P_n [58–60], and Rivier has suggested that von Neumann's law may be valid for averages as a *consequence* of Lewis's law, even when von Neumann's law is not valid for individual cells, as is the case for some cellular structures [61–63].

On the other hand, the general validity of Lewis's law has been questioned on the basis of experimental evidence: In [11] and [35] it is concluded that Lewis's law is valid only for biological tissues which have a constrained area distribution, while for coarsening froths and grain patterns it is the average *perimeter* of cells with a given number of neighbors which is proportional to that number. Iglesias and de Almeida [33] have given a maximum entropy argument for such a perimeter law

$$\langle x\rangle_n \propto n^2. \tag{41}$$

Herdtle and Aref have addressed the issue in their simulations of the ideal, dry froth and found that first degree polynomials in n fitted average areas *and* average perimeters, though perimeters were fitted slightly better, especially for small-n values [25]. It is important to realize here that experimental as well as simulation results are limited to a finite range of n values and by error bars that grow rapidly with n. So Lewis's law *could* in principle be the correct law asymptotically for large n, while at the same time a fit to available data could favor a perimeter law. We shall argue that this is indeed the case.

First, we observe the obvious: Lewis's law (40) *cannot* be valid for *small* values of n in cases where α is so large that the right-hand side becomes negative. This is the situation for froths. So if Lewis's law is generally valid, it must be for *large* values of n, where the specific meaning of "large" presumably depends on the value of α in (40). In the cases studied by Lewis, α is so small that all values for n encountered are large. Thus he found his law. For coarsening froths and grain patterns, α is larger, hence so are the values for n where the law can be valid—with the unfortunate consequence that there is not sufficient experimental and simulation data to decide for or against it. It is a definite advantage of our random-neighbor model that it allows us to *prove* that Lewis's law *is* valid as an asymptotic law at large n. Before we do that, we must clarify where we stand on another issue, however; that of what we consider fundamental to the model, and what are derived properties.

For soap froths, the fundamental dynamics is known, and von Neumann's law is an exact consequence of it, valid for each individual bubble. Statistical statements like Lewis's law are consequences of this dynamics, and should be derived from it as such, when possible. As elegant as maximum entropy arguments are, they are incomplete and may go wrong when they neglect dynamics. It is, after all, the *dynamics* of the froth that gives the entropy a chance to grow and become maximal—within whatever constraints the dynamics impose on this maximization process. And, as we shall see in the next section and in the Appendix, it is a question of major interest what signatures are left by the dynamics on the distributions found in the asymptotic scaling state.

Our master equation represents the fundamental dynamics of the soap froth only through one of its consequences, von Neumann's law. Thus, from our point of view, Lewis's law is a consequence of von Neumann's law. Entropy maximization does play a role in obtaining this consequence, since it is at the attractive fixed point for the master equation that we obtain Lewis's law. But it is the entropy of the functions $[f_n(x)]_{n=0,1,2,\ldots}$ that is maximized, and under the constraint that they obey the time-independent master equation, i.e., essentially the constraints of von Neumann's law and Euler's theorem. So *they* are fundamental, and Lewis's law is a consequence.

Now the proof: By multiplying both sides of Eq. (16) by x and integrating over x, we find

$$\begin{aligned}\bar{A}\frac{d}{dt}(P_n\langle x\rangle_n) = {} & (n-6)P_n - (c_+ + c_-)nP_n\langle x\rangle_n \\ & + c_+(n-1)P_{n-1}\langle x\rangle_{n-1} \\ & + c_-(n+1)P_{n+1}\langle x\rangle_{n+1}.\end{aligned} \tag{42}$$

Using the asymptotic form (31) for P_n, we find at the fixed point

$$0 = n - 6 - (c_+ + c_-)n\langle x\rangle_n + c_-\left(n - \frac{\dot{\bar{A}}}{c_- - c_+} - \dot{\bar{A}}(\dot{\bar{A}} - c_- + c_+)c_+(c_- - c_+)^{-3}/n\right)\langle x\rangle_{n-1}$$
$$+c_+\left(n + \frac{\dot{\bar{A}}}{c_- - c_+} + \dot{\bar{A}}(\dot{\bar{A}} - c_- + c_+)c_-(c_- - c_+)^{-3}/n\right)\langle x\rangle_{n+1} + O(1/n), \tag{43}$$

which is solved by

$$\langle x\rangle_n = \alpha(n-6) + \beta + O(1/n) \tag{44}$$

with

$$\alpha = \frac{1}{\dot{\bar{A}} + c_- - c_+}, \quad \beta = \alpha\left(\frac{c_- + c_+}{c_- - c_+} - \frac{6(c_- - c_+)}{\dot{\bar{A}}}\right). \tag{45}$$

Equation (44) shows that Lewis's law only is an asymptotic law, valid for large n.

Figure 9(a) shows our results for $\langle x\rangle_n$. Lewis's law is seen to be well obeyed for $n \geq 6$, while a perimeter law would appear as a quadratic form in this plot and definitely not fit our results. Figure 9(b) compares our results for $\langle x\rangle_n$, shown as black squares, with averaged experimental results for froths with helium gas (diamonds) and air (circles). The data were taken from tables given in [35] and [11]. Unfortunately these sources give no error bars for the numbers plotted. But if we take the differences between the two sets of experimental data as indicators for the size of error bars, we see that there is full agreement between our theory and experiments for $n \geq 5$. The total agreement between the three sets of data for $n = 6$ is due to the normalization convention used: $\langle x\rangle_6 = 1$. The very fine agreement between theory and experiments at $n = 10$ and $n = 11$ must be coincidental if the differences between the two sets of experimental data really do indicate the experimental error, because we expect this error to increase with n for $n \geq 6$. No experimental result was given in [35] for the helium froth and $n = 10$.

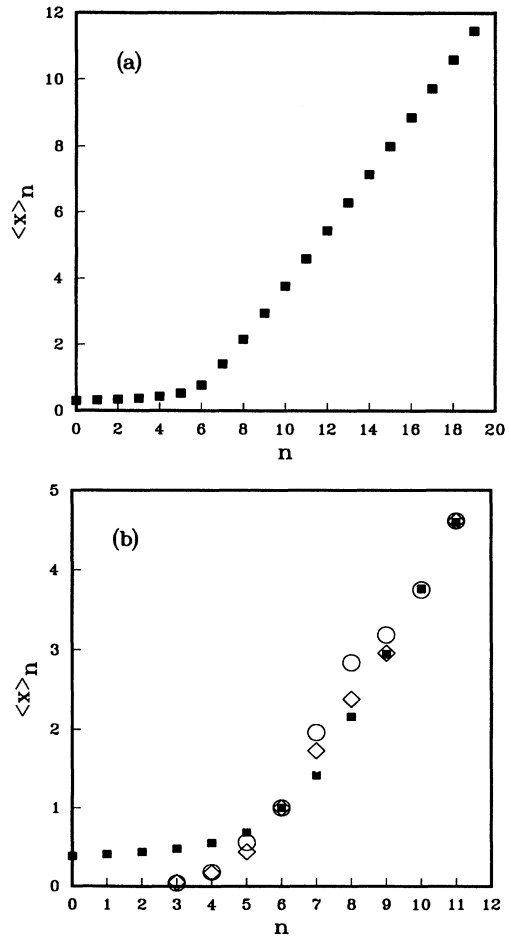

FIG. 9. (a) $\langle x\rangle_n$ vs n from the random neighbor model. (b) $\langle x\rangle_n/\langle x\rangle_6$ vs n. Black squares show the results of the random-neighbor model. Averaged experimental results for froths with helium gas (air) are shown as diamonds (circles) [35, 11]. There is no result for helium at $n = 10$.

The disagreement between theoretical and experimental results at low values of n is due to failure of the theory in predicting $\langle x\rangle_n$ correctly. This quantity is particularly sensitive to our permitting bubbles with $n = 0$, 1, and 2. The negligible probabilities that such bubbles occur within our model do not suppress $\langle x\rangle_n$, because $\langle x\rangle_n$ is the average *within* the topological class n.

We conclude the following.

(i) On the basis of experimental evidence, Lewis's law is *not* valid for all systems for *all* values of n.

(ii) The same experimental evidence cannot exclude the possibility that Lewis's law is valid for all systems *asymptotically, for n large,* with some systems demonstrating asymptotic behavior already at small values of n—such systems must have small values for α in (40), and include those studied by Lewis.

(iii) Our random-neighbor model has as a consequence that Lewis's law *is* valid asymptotically for n large.

X. THE DISTRIBUTION OF AREAS $f(x)$

By summing over n on both sides of Eq. (16), one obtains an equation for the frequency $f(x;t)$ of relative area x at time t,

$$\bar{A}\frac{\partial}{\partial t}f(x;t) = \left[\left[-(\langle n\rangle_x - 6) + \dot{\bar{A}}x\right]\frac{\partial}{\partial x} + 2\dot{\bar{A}} - \frac{\partial\langle n\rangle_x}{\partial x}\right]f(x;t). \tag{46}$$

This equation has as a stationary solution

$$f(x) = \exp(-x), \tag{47}$$

provided

$$\langle n\rangle_x = \check{A}(x-1) + 6. \tag{48}$$

This solution is interesting because it maximizes the entropy of $f(x)$ under the constraints (21) and (23) [62, 63, 33]. We know, of course, that the distribution of areas we are considering is the result of a complicated dynamical process described by Eq. (16). We *may* obtain its fixed-point solution by entropy maximization, since that is precisely what a Markov process does for us, but, as discussed in Sec. IX, the entropy to be maximized is not that of $f(x)$, but of $f_n(x)$. And in addition to the constraints (21) and (23) there are other constraints: the average topology must be 6, and the stationary versions of the infinite set of coupled equations (16) must also be satisfied. So maximum entropy *methods* are of no practical use to us: there are too many constraints, a countable infinity for every value of x.

Still we may ask whether the details of the dynamics contained in Eq. (16) leave a signature on the fixed-point distribution $f(x)$? Or do the dynamics "mess up" $f(x)$ maximally? As solution (47) to Eq. (46) shows, the last possibility requires $\langle n\rangle_x = \check{A}(x-1)+6$. Now, $\langle n\rangle_x$ has its own equation derived from Eq. (16), which it must satisfy. But that equation *is* satisfied by $\langle n\rangle_x = \check{A}(x-1)+6$, provided $\langle n^2\rangle_x - \langle n\rangle_x^2 = (c_- - c_+)(\check{A}x+6) - \check{A}^2$. And so on: $\langle n^2\rangle_x$ must satisfy an equation, which *is* satisfied by the form just given, provided $\langle n^3\rangle_x$ is a particular third degree polynomial in x.

Our numerical solution of Eq. (16) shows a small difference between $f(x)$, shown as a fully drawn line in Fig. 10(a), and $\exp(-x)$, shown as the dashed line. Figure 10(b) shows our numerical results for $\langle n\rangle_x$ vs $6 - \check{A} + \check{A}x$, and $(\langle n^2\rangle_x - \langle n\rangle_x^2 + \check{A}^2)/(c_- - c_+)$ versus $6 + \check{A}x$. The two graphs in Fig. 10(a) are so close that one may fail to distinguish between them in a numerical solution based on Monte Carlo simulation [30, 46, 49], or in experimental data [[49], Figs. 2–6]. Their difference is important, though, conceptually and practically. The differences between the fully drawn and dashed curves in Fig. 10(b) are even smaller and typically more difficult to distinguish in simulation results, because $\langle n\rangle_x$ and $\langle n^2\rangle_x - \langle n\rangle_x^2$ have larger error bars than $f(x)$ when calculated from the same data set.

The difference between the two graphs in Fig. 10(a) is of practical importance, because *if* $f(x) = \exp(-x)$ had been valid, we could have obtained the form of Eq. (16)'s fixed-point solution *analytically*. This is demonstrated in Appendix B. Since $f(x)$ differs little from $\exp(-x)$, one may instead consider using the analytical results from the appendix as a starting point for an analytical approximation scheme for the solution to Eq. (16).

Conceptually, the difference between the two graphs in Fig. 9(a) is important, because it shows that the particular dynamics of the coarsening process *has* left a signature on $f(x)$. It is actually possible to see this small difference between $f(x)$ and $\exp(-x)$ in experimental data for coarsening 2D aluminum polycrystals plotted in [[49],Fig. 2–6]. So our random-neighbor model throws light on old data. Conversely, the agreement between data and model on this subtle point shows we have invented a realistic model.

Experiments with soap froths have not yet provided data that can resolve the difference between $\exp(-x)$ and $f(x)$. Both functions fully agree within experimental errors with the experimental result in Fig. 17 of Ref. [11]. The precision it takes to resolve this difference is a new target for such experiments. Since our random-neighbor model replaces nearest-neighbor correlations with randomness, our result is presumably closer to the maximum entropy distribution $\exp(-x)$ than the exact function $f(x)$ of an ideal 2D froth is. So it may require *less* experimental precision to distinguish $f(x)$ from $\exp(-x)$ than Fig. 10 indicates.

In general, whatever the functions $f(x)$ and $\langle n\rangle_x$ are, they are related to each other by the fixed-point version of Eq. (46). That is an ordinary differential equation,

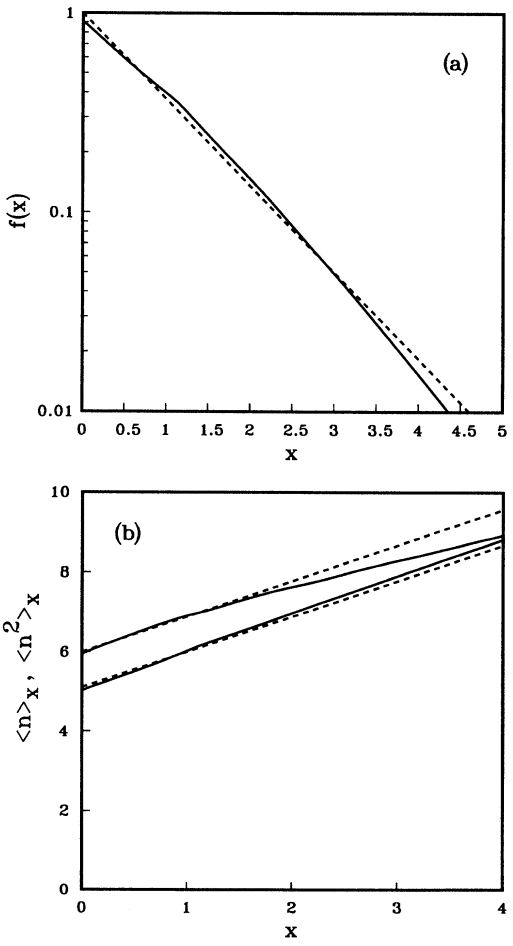

FIG. 10. (a) $f(x)$ vs x (fully drawn curve) and $\exp(-x)$ vs x (dashed curve). (b) $\langle n\rangle_x$ vs x (lower fully drawn curve) and $6 - \check{A} + \check{A}x$ vs x (lower dashed curve). $(\langle n^2\rangle_x - \langle n\rangle_x^2 + \check{A}^2)/(c_- - c_+)$ vs x (upper fully drawn curve) and $6 + \check{A}x$ vs x (upper dashed curve).

solved by

$$\langle n\rangle_x = 6 + \dot{\bar{A}}x - \dot{\bar{A}}/f(x)\int_x^\infty dx' f(x'). \tag{49}$$

This equation may be inverted to give

$$f(x) = \frac{\dot{\bar{A}}}{6 + \dot{\bar{A}}x - \langle n\rangle_x}\exp\left(-\int_0^x dx' \frac{\dot{\bar{A}}}{6 + \dot{\bar{A}}x' - \langle n\rangle_{x'}}\right), \tag{50}$$

which shows $\langle n\rangle_x < 6 + \dot{\bar{A}}x$ for all $x \geq 0$

XI. T_1 PROCESSES AND SIDE-SHEDDING

Our random-neighbor model is based on two approximations: (1) neighbor relations are random, and (2) neighbor switching T_1 processes, as shown in Fig. 2(b), do not occur. The last approximation has a dual motivation. (a) Experimentally, it is observed that T_1 processes that are unrelated to vanishing processes make up less than 1% of all topology changing processes, T_1 *and* T_2 [38]. (b) Theoretically, we notice that even if T_1 processes cause side shedding in a bubble that shrinks to vanish, they leave no apparent effect once the bubble has disappeared.

In a recent article, Fradkov *et al.* discuss under which conditions bubbles may shrink without shedding sides [32]. Working with plausible assumptions, they find that a rather symmetric geometry of a shrinking bubble suffices. Since such a geometry typically has a lower energy than an asymmetric one, the dynamics of a froth favors such geometries, thereby suppressing side shedding.

On the other hand, Stavans and Glazier [1] observed that only 16% of shrinking pentagons disappear directly [64] and only 50% of shrinking quadrangles do so according to Glazier, Gross, and Stavans [38]. Herdtle and Aref report a frequency ratio of $T1$ to $T2$ processes of 3:2 in the scaling state, as investigated in their state-of-the-art defining simulations of the ideal, dry 2D froth [25]. They also provide a rough and simple explanation of this ratio, which assumes that no four- or five-sided bubbles disappear directly, but only through side shedding to three-sided bubbles which then disappear.

However, even when side shedding occurs, it may not affect the precision of our model. As exemplified by Fig. 11 compared with the vanishing pentagon in Fig. 2(a), side shedding by a shrinking bubble does not affect the net result left over when the bubble has vanished. Of course, this net result is obtained faster when shrinking bubbles shed sides, because fewer-sided bubbles shrink faster. But if it is only at *small* areas x that side shedding sets in, only a small fraction of the bubbles in the froth are affected, and only for the short while that it takes the shrinking and shedding bubble to vanish. So $f_n(x)$ may very well change little because of side shedding, except at small values of x. All this is just hypothesizing, of course.

It is unfortunate that Herdtle and Aref report no results for the distributions $f_n(x)$, since such results could replace hypothesis with facts. Experimental results for grain growth in aluminum, Figs. 2–4 in [49], show a difference to our results for $f_n(x)$ for $n = 4$, 5, and 6 and $x \sim 0$, which could well be explained as the result of side shedding. The functions seem to vanish as x approaches 0. However, one should not uncritically identify grain growth with coarsening in froths; especially not when side shedding is in focus. The fast and the slow dynamics in froths occur on the same time scale in grain growth, and domain boundaries in grain growth may consequently deviate from the perfect arcs of circles they form in froths. The question of side shedding is particularly sensitive to this difference between the two systems. Also, recent experiments on 2D grain growth in thin polycrystalline films of succininitrile show four- and five-sided grains shrinking almost to the vanishing limit without shedding sides [12]. These experimental results are in accord with computer simulations of single, shrinking grains, presented in the same article.

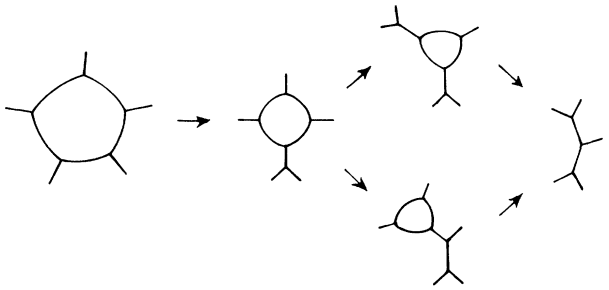

FIG. 11. Side shedding by T_1 process in a shrinking bubble. Compare the result with Fig. 2(a).

So all we can conclude about side shedding for the present is that it is under investigation, and that it should be investigated also in direct simulations of ideal, dry froths. But this lack of hard facts does not affect our model building in the present paper. Our goal was a minimal model, and we have arrived at that goal. Side-shedding may then be added to this minimal model, as done by Fradkov and Udler in their model [49], for example. On the basis of their results, we expect side shedding to increase the ratio P_5/P_6 towards the experimental values shown in Fig. 8(b).

XII. CONCLUSIONS, SUGGESTIONS

We have described a minimal model for the ideal, dry, 2D froth and seen that the single-bubble distributions $f_n(x;t)$ to a good approximation form a complete set of variables, sufficient to describe the dynamics of these variables. von Neumann's law and Euler's theorem for the plane, supplemented with a random-neighbor approximation, give a closed and complete set of dynamical equations for these distributions. These equations have a unique attractive fixed point for their time evolution. At this fixed point, we found normal growth with exponent 1/2. We also found the asymptotic n dependence of P_n and $\langle x\rangle_n$ analytically. The latter result amounts to an analytical proof of Lewis's law, and shows that it is an

asymptotic law. That is one important result obtained with our model.

We found $f_n(x) = \lim_{t\to\infty} f_n(x;t)$ numerically, and see a major analytical challenge in our master equation: it is sufficiently simple to invite speculations about its analytical solvability at the attractive fixed point. Appendix B gives some ideas and our results from a first attempt of an analytical solution. It is based on the ansatz $f(x) = \exp(-x)$, a form suggested by experimental as well as simulation results. It is, however, another important result of the present paper that $f(x) \neq \exp(-x)$. We find that directly, numerically, and we find it indirectly, analytically, in Appendix B. The difference between $\exp(-x)$ and our $f(x)$ is not big—14% on the second moment $\langle(x-1)^2\rangle$—but the difference to the exact distribution $f(x)$ for an ideal, dry, 2D froth is presumably bigger. Existing results from direct simulations of this system do not resolve this difference. This is a challenge waiting to be met. Neither do existing experimental results for 2D soap froths. That is another challenge. Experimental results for 2D grain growth in aluminum show the same qualitative difference between $f(x)$ and $\exp(-x)$ as our $f(x)$ does. There might, of course, be other reasons why these experiments give the function $f(x)$ that they do, reasons related to the experimental situation or reasons stemming from the difference between grain growth and coarsening froths. But it would be interesting to reanalyze these experimental results in light of our findings for $f(x)$.

With further model building in view, it would be interesting if direct numerical simulations of the ideal, dry, 2D froth could be pushed to a precision, where the distributions $f_n(x)$ could be given, and the role and rates of T_1 processes elucidated for individual topological classes. In particular, it would be interesting to understand the conditions for, and rates of, side shedding in shrinking bubbles. Potts model simulations have already given $f_n(x)$, but with large statistical errors, and these lattice simulations are ill suited to the study of T_1 processes in ideal froths. The same questions are, of course, at least as interesting to study experimentally in dry 2D froths. Existing results for $f_n(x)$ demonstrate that these functions can be obtained. It is "merely" better statistics that is needed.

On the theoretical side, we see several directions in which we can extend the work presented here. What we presented above we regard as a minimal model. Considering how well it already agrees with experiments, it might be rewarding to refine it, with an eye on what was left out in its minimal version. That was correlations and T_1 processes. So one may contemplate the following extensions.

(1) Instead of choosing neighbors to vanishing domains at random with bias $n/6$, one may choose them with a more realistic bias, one that takes into account the topology of the vanishing domain, and results in Aboav-Weaire's law. In this way Aboav-Weaire's law is built into the model by hand, but it remains a random-neighbor model. What is interesting is how this change affects $f_n(x)$ and P_n. Will they, as one would expect, agree even better with experiments than they already do?

(2) One may add terms describing $T1$ processes, side shedding in particular. Such terms should preferably have a form based on general arguments and rates that are determined dynamically to make their addition more than a mere *ad hoc* adjustment. Taking $T1$ processes and side shedding into account needs not interfere with the random-neighbor approximation.

(3) The random-neighbor model may presumably be used as the starting point for a systematic perturbation theory that takes correlations into account. Correlations are of secondary importance for the functions $f_n(x)$, judging from how well we can describe them with a model neglecting correlations. Experimentally, one has not been able to measure correlations beyond the nearest-neighbor correlations expressed in Aboav-Weaire's law. So one correction term may be all that is needed to obtain full agreement with experimental results.

(4) At least as interesting is the question of coarsening and domain growth in *three* dimensions. The higher dimension gives a larger average number of neighbors to bubbles. This should make the random-neighbor approximation even better than in two dimensions. There is, however, no known equivalent to von Neumann's law in three dimensions. References [31], [23], and [26] give results that point towards an approximate substitute.

(5) Our model for soap froths may be adapted to describe and interpret the dynamics of other domain boundary networks in 2D. It has been used successfully to model domain pattern dynamics in magnetic garnet film [65]. We already mentioned grain growth in aluminum. Grain growth in other materials are obvious cases. So is the bubble pattern in the liquid-gas coexistence region of monolayers studied in [8].

In summary, the random-neighbor model that was presented here agrees so well with experimental and simulation data that it should be refined, as suggested. As it stands, the model has already helped clarify the status of Lewis's law, and presents some challenges to the precision of experiments and computer simulations. It also suggests a reanalysis of experimental data on grain growth in aluminum. Refined versions of the model will surely present even stronger challenges, but may also require better data to guide the model building.

ACKNOWLEDGMENTS

I thank Bernard Derrida, Per C. Hemmer, and Ole G. Mouritsen for their stimulating interest in the work presented here, and M. P. Anderson and J. A. Glazier for permission to use figures from their articles. The Danish Natural Science Research Council supported this work through Grant No. 11-9450-1.

APPENDIX A: NOTATIONS

This appendix collects our notation, which was introduced gradually through the paper wherever needed for the first time.

A bubble's *topology* n is just its number of neighbors. $p_n(A;t)$ denotes a froth's relative frequency of bubbles

with area A and topology n at time t. $\bar{A}$ is the average area at time t, and $\dot{\bar{A}}$ its rate of change. $x = A/\bar{A}$ is a relative measure of area. $f_n(x;t) = \bar{A}p_n(A;t)$ is dimensionless, and independent of t in the scaling state of normal growth. That gives rise to the notation

$$f_n(x) = \lim_{t\to\infty} f_n(x;t). \tag{A1}$$

c_+ and c_- are one-sixth of the rates for positive and negative change in topology, respectively, and are given in dimensionless form in Eq. (17).

P_n is the fraction of bubbles with topology n, and is called the topological distribution, or side distribution, since n is also the number of sides in such bubbles,

$$P_n = P_n(t) = \int_0^\infty dA\, p_n(A;t) = \int_0^\infty dx\, f_n(x;t). \tag{A2}$$

$f(x;t)$ is the fraction of bubbles having relative area x,

$$f(x;t) = \sum_{n=0}^{\infty} f_n(x;t). \tag{A3}$$

The moments of the topological distribution are called topological moments,

$$\mu_0 = \sum_{n=0}^{\infty} P_n = 1, \tag{A4}$$

$$\mu_1 = \sum_{n=0}^{\infty} nP_n = 6, \tag{A5}$$

$$\mu_m = \sum_{n=0}^{\infty} (n-6)^m P_n \quad \text{for} \quad m \geq 2. \tag{A6}$$

The average relative area is written

$$\langle x\rangle = \int_0^\infty dx\, xf(x;t) = 1. \tag{A7}$$

The average relative area for a given topology is written as

$$\langle x\rangle_n = \int_0^\infty dx\, xf_n(x;t)/P_n, \tag{A8}$$

and the topological moments for a given relative area is written

$$\langle n\rangle_x = \sum_{n=0}^{\infty} nf_n(x;t)/f(x;t), \tag{A9}$$

$$\langle n^m\rangle_x = \sum_{n=0}^{\infty} n^m f_n(x;t)/f(x;t). \tag{A10}$$

APPENDIX B: ANALYTIC SOLUTION AT FIXED POINT?

In this appendix we demonstrate that if one *assumes* that $f(x) = \exp(-x)$, then one can find exact analytical expressions for all the functions $f_n(x)$. These expressions contain three numerical constants, c_+, c_-, and $\dot{\bar{A}}$ which must be determined from nonlinear self-consistency conditions. We have not been able to find any solution to these conditions. They are violated by a few per mil, when they are closest to being fulfilled. If one can prove analytically that there is no solution, one has proven that $f(x) \neq \exp(-x)$. That we know already from our numerical solution, so it is maybe not so interesting. More interesting is the observation that $\exp(-x)$ is a good approximation to the exact numerical result for $f(x)$. So we believe that an efficient perturbative solution may be formulated, using our analytical expressions for $f_n(x)$ as the leading-order approximation. We have not tried this out, and here just demonstrate how to find $f_n(x)$ for given $f(x)$.

To this end we introduce the generating function

$$f(x,y) = \sum_{n=0}^{\infty} y^n f_n(x), \tag{B1}$$

and find from the fixed-point version of Eq. (16) that $f(x,y)$ must satisfy the equivalent equation

$$0 = \left[(6 + \dot{\bar{A}}x)\frac{\partial}{\partial x} + 2\dot{\bar{A}} + \left\{ c_-(1-y) - c_+y(1-y) - y\frac{\partial}{\partial x} \right\} \frac{\partial}{\partial y} \right] \times f(x,y). \tag{B2}$$

This is a partial-differential equation of second order, which we must solve on the strip

$$\{(x,y)|\, 0 \leq x\ ,\ \ 0 \leq y \leq 1\}.$$

Inspection of Eq. (B2) shows that a solution is determined by its value for $y = 1$ and its behavior at $x \to \infty$. For $y = 1$

$$f(x,1) = \sum_{n=0}^{\infty} f_n(x) \equiv f(x), \tag{B3}$$

which is the frequency with which the relative area x occurs in the ensemble *irrespective* of its topology.

By an inverse Laplace transform we turn Eq. (46) into a *first-order* partial-differential equation: writing

$$f(x,y) = \int_0^\infty d\xi \exp(-x\xi)\tilde{f}(\xi,y), \tag{B4}$$

Eq. (B2) becomes equivalent with

$$0 = \left[-6\xi - \dot{\bar{A}}\xi\frac{\partial}{\partial\xi} + \dot{\bar{A}} + \left\{ c_-(1-y) - c_+y(1-y) + y\xi \right\} \frac{\partial}{\partial y} \right] \tilde{f}(\xi,y). \tag{B5}$$

This equation is solved by the method of characteristics. Writing

$$\tilde{f}(\xi,y) = \xi\exp(-6\xi/\dot{\bar{A}})g(\xi,y), \tag{B6}$$

the function g is constant on lines $[\tilde{\xi}(y), y]$ in the (ξ, y) plane which satisfy the ordinary first-order differential

equation

$$\frac{d\tilde{\xi}}{dy} = \frac{-\dot{A}\tilde{\xi}}{c_-(1-y) - c_+ y(1-y) + y\tilde{\xi}}, \tag{B7}$$

i.e., $g(\xi, y) = g(\xi_1, 1)$, where $\xi_1 = \xi_1(\xi, y)$ is the value $\tilde{\xi}(1)$ for the solution to (B7) passing through (ξ, y). Inserting in (B6) and (B4), we find

$$f(x,y) = \int_0^\infty d\xi \exp(-x\xi)\xi/\xi_1 \times \exp[6(\xi_1 - \xi)/\dot{A}]\tilde{f}(\xi_1, 1), \tag{B8}$$

which gives $f(x, y)$, and therefore $f_n(x)$, in terms of (the inverse Laplace transform of) $f(x)$. In general this expression may be too complicated to be useful, since we cannot solve (B7) analytically. It is equivalent to a Riccati equation. But in the special case of $f(x) = \exp(-x)$ we have $\tilde{f}(\xi_1, 1) = \delta(\xi_1 - 1)$, so there is only one characteristic line on which $\tilde{f}(\xi, y)$ has support, the one passing through $(\xi, y) = (1, 1)$. Consequently, Eq. (B8) gives

$$f(x,y) = (\text{function of } y)\exp[-x\tilde{\xi}(y)] \tag{B9}$$

from which follows

$$f_n(x) = \frac{1}{n!}\left(\frac{\partial}{\partial y}\right)^n_{y=0} f(x,y) = \mathcal{P}_n(x)\exp(-\xi_0 x), \tag{B10}$$

where $\xi_0 = \tilde{\xi}(0)$, and $\mathcal{P}_n(x)$ is a polynomial of degree n in x. Now that we have proven that $f_n(x)$ has the form just given, these functions are most easily determined from the original equation (16) in its time-independent version. Solved for $f_{n+1}(x)$, it gives the recursion relation

$$f_{n+1}(x) = \frac{-1}{c_-(n+1)}\left\{\left[[-(n-6) + \dot{A}x]\frac{\partial}{\partial x} + 2\dot{A} - (c_+ + c_-)n\right] f_n(x;t) + c_+(n-1)f_{n-1}(x;t)\right\}, \tag{B11}$$

which is initialized with

$$f_{-1}(x) = 0, \tag{B12}$$

$$f_0(x) = f_0(0)\exp(-\xi_0 x). \tag{B13}$$

Throughout the calculations leading to these expressions we have treated c_+, c_-, and $\dot{A}$ as free parameters. Now they must be determined self-consistently from their definitions (17) and (18), while $f_0(0)$ in (B13) is determined from the normalization condition (21). As mentioned in the beginning of this appendix, we have not been able to determine self-consistent values for c_+ and c_-. This suggests $f(x) \neq \exp(-x)$. On the other hand, we found the relative violation of the self-consistency conditions to be small. This suggests, as does direct inspection of Fig. 10, that the form $\exp(-x)$ is a good approximation to the exact solution.

* Electronic address: flyvbj@nbivax.nbi.dk

[1] J. Stavans and J. A. Glazier, Phys. Rev. Lett. **62**, 1318 (1989).
[2] J. A. Glazier and J. Stavans, Phys. Rev. A **40**, 7398 (1989).
[3] J. Stavans, Phys. Rev. A **42**, 5049 (1990).
[4] D. J. Durian, D. A. Weitz, and D. J. Pine, Science **252**, 686 (1991).
[5] D. J. Durian, D. A. Weitz, and D. J. Pine, Phys. Rev. A **44**, R7902 (1992).
[6] G. Helgesen and Arne T. Skjeltorp, in *Random Fluctuations and Pattern Growth: Experiments and Models,* edited by H. Stanley and N. Ostrowsky, Vol. 157 of *NATO Advanced Study Institute Series E: Applied Science* (Kluwer Academic, Boston, 1988).
[7] K. J. Stine, S. A. Rauseo, B. G. More, J. A. Wise, and C. M. Knobler, Phys. Rev. A **41**, 6884 (1990).
[8] B. Berge, A. J. Simon, and A. Libchaber, Phys. Rev. A **41**, 6893 (1990).
[9] K. L. Babcock and R. M. Westervelt, Phys. Rev. A **40**, 2022 (1989); Phys. Rev. Lett. **64**, 2168 (1990).
[10] K. L. Babcock, R. Seshadri, and R. M. Westervelt, Phys. Rev. A **41**, 1952 (1990).
[11] J. A. Glazier, M. P. Anderson, and G. S. Grest, Philos. Mag. B **62**, 615 (1990).
[12] V. E. Fradkov, M. E. Glicksman, M. Palmer, J. Nordberg, and K. Rajan (unpublished).
[13] J. C. M. Mombach, M. A. Z. Vasconcellos, and Rita M. C. de Almeida, J. Phys. D **23**, 600 (1990).
[14] J. C. M. Mombach, R. M. C. de Almeida, and J. R. Iglesias, Phys. Rev. E **47**, xxxx (1993).
[15] J. C. M. Mombach, Rita M. C. de Almeida, and J. R. Iglesias (to be published).
[16] D. Weaire and Hou Lei, Philos. Mag. Lett. **62**, 427 (1990).
[17] D. Weaire and V. Pageron, Philos. Mag. Lett. **62**, 417 (1990).
[18] F. Bolton and D. Weaire, Phys. Rev. Lett. **65**, 3449 (1990).
[19] F. Bolton and D. Weaire, Philos. Mag. B **63**, 795 (1991).
[20] F. Bolton and D. Weaire, Philos. Mag. B **65**, 473 (1992).
[21] D. Weaire, F. Bolton, P. Molho, and J. A. Glazier, J. Phys. Condens. Matter 3, 2101 (1991).
[22] K. Kawasaki and Y. Enomoto, Physica A **150**, 462 (1988); K. Kawasaki, T. Nagai, and K. Nakashima, Philos. Mag. B **60**, 399 (1989); K. Kawasaki, Physica A **163**,

59 (1990).
[23] M. P. Anderson, G. S. Grest, and D. J. Srolovitz, Philos. Mag. B **59**, 293 (1989).
[24] E. A. Holm, J. A. Glazier, D. J. Srolovitz, and G. S. Grest, Phys. Rev. A **43**, 2662 (1991).
[25] T. Herdtle and H. Aref, J. Fluid Mech. **241**, 233 (1992).
[26] J. A. Glazier, Phys. Rev. Lett. **70**, 2170 (1993).
[27] N. Ryum and O. Hunderi, Acta Metall. **37**, 1375 (1989); **37**, 1381 (1989).
[28] J. Stavans, E. Domany, and D. Mukamel, Europhys. Lett. **15**, 479 (1991).
[29] M. A. Peshkin, K. J. Strandburg, and N. Rivier, Phys. Rev. Lett. **67**, 1803 (1991).
[30] H. Flyvbjerg and C. Jeppesen, Phys. Scr. **T38**, 49 (1991).
[31] J. E. Avron and D. Levine, Phys. Rev. Lett. **69**, 208 (1992).
[32] V. E. Fradkov, M. O. Magnasco, D. Udler, and D. Weaire, Philos. Mag. Lett. **67**, 202 (1993).
[33] J. R. Iglesias and Rita M. C. de Almeida, Phys. Rev. A **43**, 2763 (1991).
[34] D. Weaire and N. Rivier, Contemp. Phys. **25**, 59 (1984).
[35] J. A. Glazier, Ph.D. thesis, Chicago University (unpublished).
[36] J. A. Glazier and D. Weaire, J. Phys. Condens. Matter **4**, 1867 (1992).
[37] H. Flyvbjerg, Physica A **194**, 298 (1993).
[38] J. A. Glazier, S. P. Gross, and J. Stavans, Phys. Rev. A **36**, 306 (1987).
[39] J. von Neumann, in *Metal Interfaces*, edited by C. Herring (American Society for Metals, Cleveland, OH, 1952), p. 108; W. W. Mullins, J. Appl. Phys. **27**, 900 (1956).
[40] D. A. Aboav, Metallography **3**, 383 (1970).
[41] D. Weaire, Metallography **7**, 157 (1974).
[42] D. A. Aboav, Metallography **13**, 43 (1980).
[43] C. J. Lambert and D. Weaire, Metallography **14**, 307 (1981); Philos. Mag. B **47**, 445 (1983).
[44] M. Blanc and A. Mocellin, Acta Metall. **21**, 1231 (1979).
[45] Most people would just call it mean-field theory. But the same approximation applied to, for example, the Ising model does not give its mean-field theory, though the difference is not essential.
[46] V. E. Fradkov, Philos. Mag. Lett. **58**, 271 (1988); V. E. Fradkov, D. G. Udler, and R. E. Kris, *ibid.* **58**, 277 (1988).
[47] M. Marder, Phys. Rev. A **36**, 438 (1987).
[48] C. W. J. Beenakker, Phys. Rev. Lett. **57**, 2454 (1986).
[49] V. E. Fradkov and D. G. Udler, Chernogolovka Report No. T-21116, 1989 (unpublished).
[50] C. W. J. Beenakker, Phys. Rev. A **37**, 1697 (1988).
[51] C. S. Smith, in *Metal Interfaces*, edited by C. Herring (American Society for Metals, Cleveland, OH, 1952), p. 65.
[52] R. L. Fullman, in *Metal Interfaces*, edited by C. Herring (American Society for Metals, Cleveland, OH, 1952), p. 179.
[53] P. S. Sahni, D. J. Srolovitz, G. S. Grest, M. P. Anderson, and S.A. Safran, Phys. Rev. B **28**, 2705 (1983).
[54] M. P. Anderson, D. J. Srolovitz, G. S. Grest, and P. S. Sahni, Acta Metall. **32**, 783 (1984).
[55] S. K. Kurtz and F. M. A. Carpay, J. Appl. Phys. **51**, 5725 (1980); **51**, 5745 (1980).
[56] F. T. Lewis, Anat. Rec. **38**, 341 (1928); Am. J. Botany **30**, 74 (1943).
[57] V. V. Smoljaninov, *Mathematical Models of Tissues* (Nauka, Moscow, 1980), Chap. 3 (in Russian).
[58] R. Kikuchi, J. Chem. Phys. **24**, 861 (1956).
[59] N. Rivier and A. Lissowski, J. Phys. A **15**, L143 (1982).
[60] For an early application of the maximum-entropy principle to the topological distribution P_n of 2D soap froth patterns, see [58].
[61] N. Rivier, Philos. Mag. B **47**, L45 (1983).
[62] N. Rivier, Philos. Mag. B **52**, 795 (1985).
[63] N. Rivier, Physica D **23**, 129 (1986).
[64] In [35] this number is given as 24% with [1] as the source.
[65] P. Bak and H. Flyvbjerg, Phys. Rev. A **45**, 2192 (1992); Physica A **185**, 3 (1992).